Electronic Supplementary Material (ESI) for Sustainable Energy & Fuels.

Supporting information

for

Mn Boosted the Electrocatalytic Hydrogen Evolution Reaction of N, P co-doped Mo_2C via Synergistically Tuning the Electronic Structure

Zongyun Mu[a, c], Ting Guo[a], Hao Fei[a], Dingsheng Xu[b], Yaoqing Mao[c], Zhuangzhi Wu[a, *], Dezhi Wang[a, *]

[a] *School of Materials Science and Engineering, Central South University, Changsha 410083, China*

[b] *Sinosteel Tianyuan Co. Ltd., Ma'anshan 241000, China*

[c] *Hunan Special Metal Materials Co. Ltd., Changsha 410013, China*

E-mail address: zwu@csu.edu.cn; dzwang@csu.edu.cn

Experiment

Materials

Phosphomolybdic acid ($H_3O_{40}PMo_{12}$), dicyandiamide (DCA) and manganese (II) acetate tetrahydrate ($Mn(CH_3COO)_2{\cdot}4H_2O$) were provided by Shanghai Aladdin Biochemical Technology. Ethanol was purchased from Beijing Chemical Corp. Nafion solution (5 wt%) was obtained from DuPont Company (USA). Sulfuric acid (H_2SO_4, 98%) was provided by Xilong Chemical Co., Ltd. All chemicals were used as received without further treatment.

Synthesis of 0.08MnNP-Mo_2C

Typically, for the synthesis of 0.08MnNP-Mo_2C, 19.6 mg (0.08 mmol) $Mn(CH_3COO)_2{\cdot}4H_2O$, 6 g DCA and 0.912 g (0.5 mmol) $H_3O_{40}PMo_{12}$ were dissolved and mixed in 100 mL ethanol by stirring at 80 °C. Next, the resulting solution was kept at 80 °C until the ethanol was completely removed, following by drying at 60 °C for 5 h. Then, the collected white precursor was first calcined at 550 °C for 4 h and then further carbonized at 800 °C for 3 h with a heating rate of 5 °C min^{-1} in argon flow. After the furnace was cooled down naturally to room temperature, the calcined precursor was ground into powder using an agate mortar and marked as 0.08MnNP-Mo_2C. With the different feeding amount of $Mn(CH_3COO)_2{\cdot}4H_2O$ from 0 to 0.16 mmol, the control samples were also synthesized at the same conditions and denoted as xMn-Mo_2C (x=0, 0.01 and 0.16 mmol).

Preparation of working electrodes

In a typical procedure, 3 mg of the as-synthesized material was dispersed in a mixture of Nafion solution (5 wt%, 80 μL), ethanol (200 μL) and distilled water (800 μL), and then ultrasonicated for 30 min to generate a homogeneous dark slurry. Next, 5 μL of the slurry was dropped onto a smooth carbon electrode with a diameter of 3 mm and dried in air for 5 h. The mass loading of catalysts was

calculated to be 0.213 mg cm^{-2}.

Characterizations

The X-ray diffraction (XRD) patterns were collected by a D/max-2500 X-ray diffractometer using a Cu Kα radiation. The morphology and microstructure were observed using FEI Sirion 200 scanning electron microscopy (SEM) and JEOL 2100F transmission electron microscope (TEM) equipped with quantitative X-ray spectroscopy capabilities for element distribution analysis. The surface compositions and element chemical states were analyzed by X-ray photoelectron spectroscopy (XPS, Thermo Fisher Scientific K-ALPHA) with an Al Ka radiation using C 1s (284.6 eV) as a reference. Brunauer-Emmett-Telle (BET) surface area and corresponding pore size distribution were determined on Quadrasorb SI-3MP with nitrogen adsorption at 77 K.

Electrochemical measurements

The electrochemical experiments were carried out in an electrochemical workstation (CHI 660E) with a three-electrode system in 0.5 M H_2SO_4. The saturated calomel electrode (SCE), as-prepared glassy carbon electrodes and a graphite rod were adopted as the reference electrode, working electrode and counter electrode, respectively. To evaluate the hydrogen evolution reaction activity, the linear sweep voltammograms (LSV) were conducted in the range from 0.1 to – 0.4 V with 2 mV s^{-1}. Electrochemical impedance spectroscopy (EIS) was implemented from 1 MHz to 1 Hz with an amplitude of 5 mV at an overpotential of 0.2 V. The cyclic voltammetry (CV) curves were collected from 0 to 0.3 V at various scan rates (20, 40, 60, 80, 100, 120 and 140 mV s^{-1}) to obtain the electrochemical double-layer capacitances (C_{dl}) and electrochemically active surface area (ECSA). The slopes k of the fitting line from current density variation plotted against scan rate curves were obtained, and $C_{dl} = k/2$.

The ECSA was calculated according to the following formula[1]:

$$A_{ECSA} = \frac{\text{electrochemical capacitance}}{40\ \mu F\ cm^{-2}\ \text{per}\ cm^2_{ECSA}}$$

The turnover frequency (TOF) was calculated by the formula below:

$$TOF = \frac{\text{no. of total hydrogen turnovers } cm^{-2} \text{ of geometric area}}{\text{no. of active sites } cm^{-2} \text{ of geometric area}}$$

The total number of hydrogen turnovers per current density was obtained using the formula:

$$\text{No. of } H_2 = (\text{per } \frac{mA}{cm^2})(\frac{1\ C\ s^{-1}}{1000\ mA})(\frac{1\ \text{mol of e}}{96485.3\ C})(\frac{1\ \text{mol of } H_2}{2\ \text{mol of e}})(\frac{6.022 \times 10^{23} H_2\ \text{molecules}}{1\ \text{mol of } H_2})$$

$$= 3.12\times10^{15}\ \frac{H_2\ s^{-1}}{cm^2}\ \text{per}\ \frac{mA}{cm^2}$$

Due to the uncertainty of real hydrogen adsorption site, the number of active sites was evaluated from the surface sites, where Mo and C atoms acted as possible active sites. Based on the roughness factor and the unit cell of Mo_2C (volume of 37.2 Å^3), the number of active sites per real surface area was deduced by the following formula:

$$no.\ of\ active\ sites = \left(\frac{2\frac{atoms}{unit\ cell}}{37.2\frac{Å^3}{unit\ cell}}\right)^{2/3} = 1.42 \times 10^{15}\ atoms\ cm_{real}^{-2}$$

Finally, plots of the current density were converted into TOF plots according to:

$$TOF = \frac{\left(3.12 \times 10^{15}\frac{H_2/s}{cm^2}\ per\ \frac{mA}{cm^2} \times |j|\right)}{\left(1.42 \times 10^{15}\ atoms\ cm_{real}^{-2}\right)A_{ECSA}}$$

The long-term stability of the catalysts was evaluated by the continuous CV scanning and

chronoamperometry. All the potentials reported in this work were referenced to a reversible hydrogen electrode based on the Nernst equation ($E_{RHE} = E_{SCE} + 0.059*pH + 0.209$) without *iR* corrections.

Computational details

The density functional theory (DFT) calculations were conducted via VASP (Vienna ab initio simulation package), and the projector-augmented plane wave pseudopotentials were adopted to process the ion-electron interactions. The electronic exchange and correlation effects were treated by the Perdew-Burke-Ernzerhof (PBE) of Generalized Gradient Approximation (GGA). The model of β-Mo_2C was constructed based on Wang's work[2]. A periodic 4 × 4 × 1 supercell with a Γ-centered 2 × 2 × 1 k-point grid was used to conduct the surface analysis and calculation in Brillouin zone. The plane-wave cutoff energy was set as 520 eV. The Mo_2C (001) surface was modeled to calculate the change in Gibbs free energy of hydrogen adsorption (ΔG_{H^*}), where 15 Å vacuum above the Mo_2C (001) surface was taken into consideration. ΔG_{H^*} was calculated according to the following equation:

$$\Delta G = E_{total}-E_{surface}-1/2E_{H2}+ \Delta E_{ZPE} - T\Delta S$$

where E_{total}, $E_{surface}$, E_{H2}, ΔE_{ZPE} and ΔS were referred to total energy for the surface with H adsorption, the surface without H adsorption, the energy of H_2 in gas phase, the zero-point energy change and the entropy change, respectively. In vaspkit 501 function mode, ΔE_{ZPE} and ΔS were calculated as G(T) on account of frequency calculation. Finally, in reference of the investigation form Nørskov[3], ΔG_{H^*} was calculated as follows:

$$\Delta G_{H^*}=\Delta E_{H^*} + 0.28\ eV$$

where $\Delta E_{H^*} = E_{total}-E_{surface}-1/2E_{H2}$.

Table S1 Calculated lattice constants and grain sizes of various samples.

Sample	Grain size / nm	Lattice constant / Å		
		a	***b***	***c***
NP-Mo_2C	5.55	3.0171	3.0171	4.7418
0.01MnNP- Mo_2C	5.53	3.0141	3.0141	4.7399
0.08MnNP- Mo_2C	5.50	3.0115	3.0115	4.7376
0.16MnNP- Mo_2C	5.48	3.0051	3.0051	4.7368

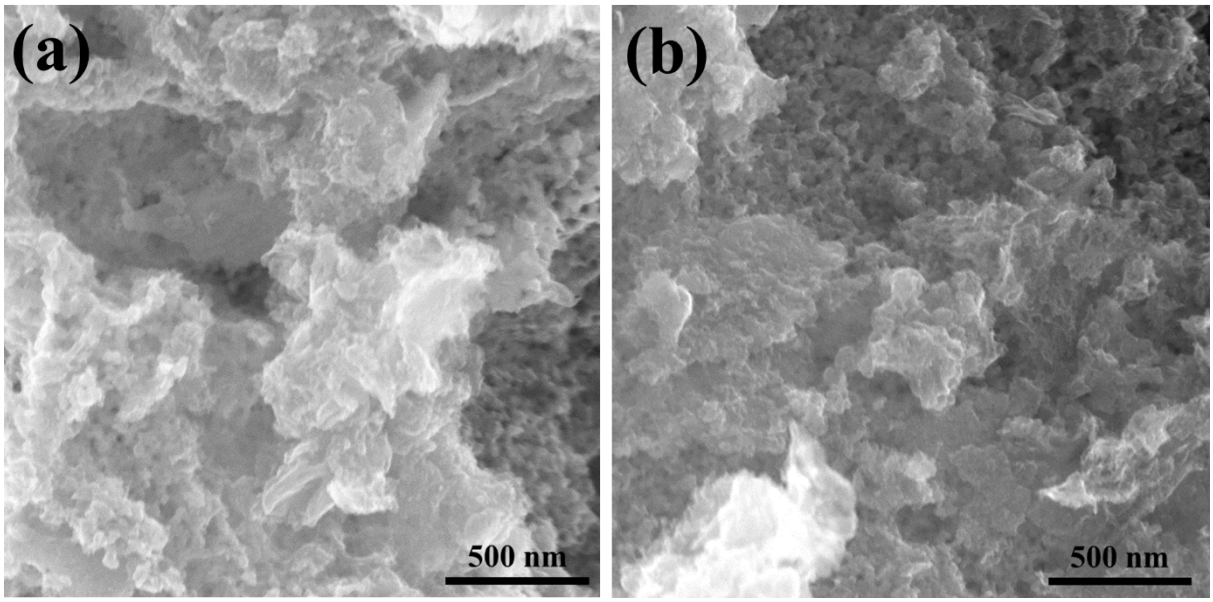

Fig. S1 SEM images of (a) NP-Mo_2C and (b) 0.08MnNP-Mo_2C.

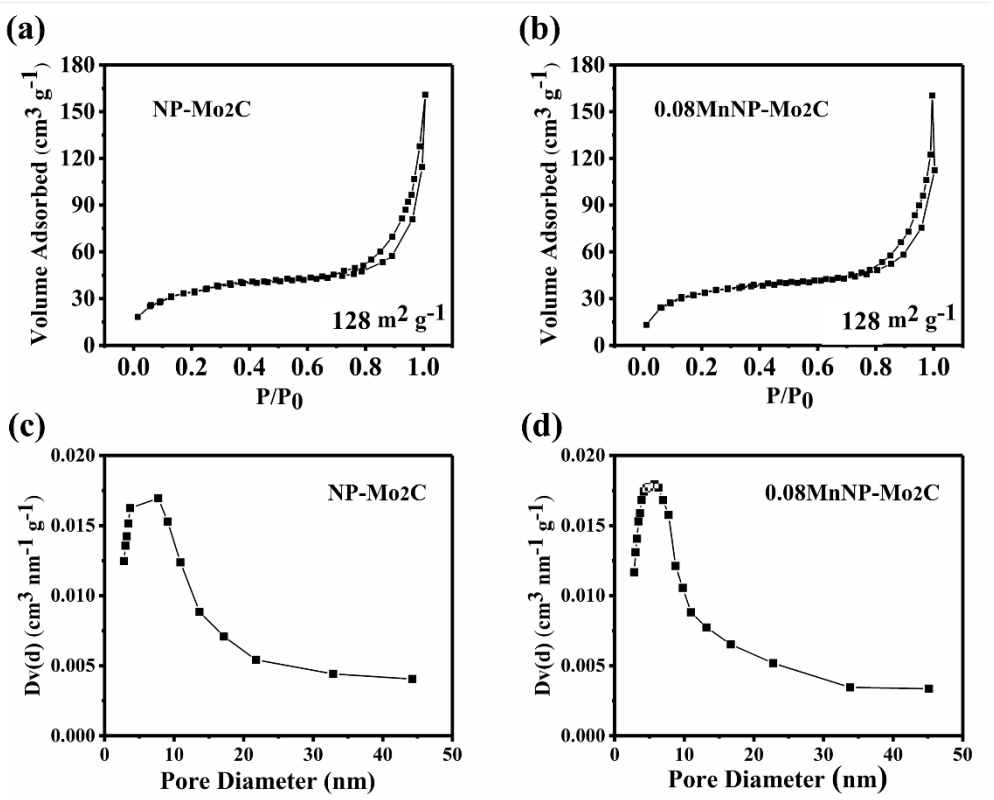

Fig. S2 Nitrogen adsorption–desorption isotherms of (a) NP-Mo_2C and (b) 0.08MnNP-Mo_2C and the corresponding pore size distributions by BJH method of (c) NP-Mo_2C and (d) 0.08MnNP-Mo_2C.

Table S2 Surface elemental compositions determined by XPS.

Sample	Mo	C	N	P	O	Mn
	wt.%	wt.%	wt.%	wt.%	wt.%	wt.%
NP-Mo_2C	46.01	43.93	3.70	2.09	4.27	0
0.01MnNP-Mo_2C	46.10	43.83	3.67	2.07	4.26	0.07
0.08MnNP-Mo_2C	45.78	43.63	3.66	2.03	4.27	0.62
0.16MnNP-Mo_2C	45.19	43.63	3.62	2.02	4.23	1.31

Table S3 Comparison of the electrocatalytic activity over 0.08MnNP-Mo_2C with other related electrocatalysts for HER in 0.5 M H_2SO_4.

Catalysts	Loading (mg cm^{-2})	Current density j (mA cm^{-2})	Overpotential at the corresponding j (mV)	Tafel slope (mV dec^{-1})	Ref
Mn, N-Mo_2C-0.01	~0.55	10	163	66	4
Mo_2N-Mo_2C/HGr-3	~0.337	10	157	55	5
Mo_2C/CNT-GR	~0.65	10	130	58	6
Mo-Mo_2C-0.077	~0.38	10	150	55	7
Mo_2C-GNR	/	10	152	65	8
Co-Mo_2C-0.020	0.14	10	140	39	9
Co-NC@Mo_2C	~0.83	10	143	60	10
Mo_2C@NC	0.5	10	36	33.7	11
uf-Mo_2C/CF-2	0.25	10	184	71	12
Mo_2C/C (2:2)	0.28	10	180	71	13
P-Mo_2C@C	1.3	10	89	42	14
N, P-Mo_2C@C	0.9	10	141	56	15
Biochar-derived Mo_2C	0.213	10	161	57	16
np-Mo_2C NWS	0.21	10	200	53	17
0.08MnNP-Mo_2C	0.213	10	167	51	This work

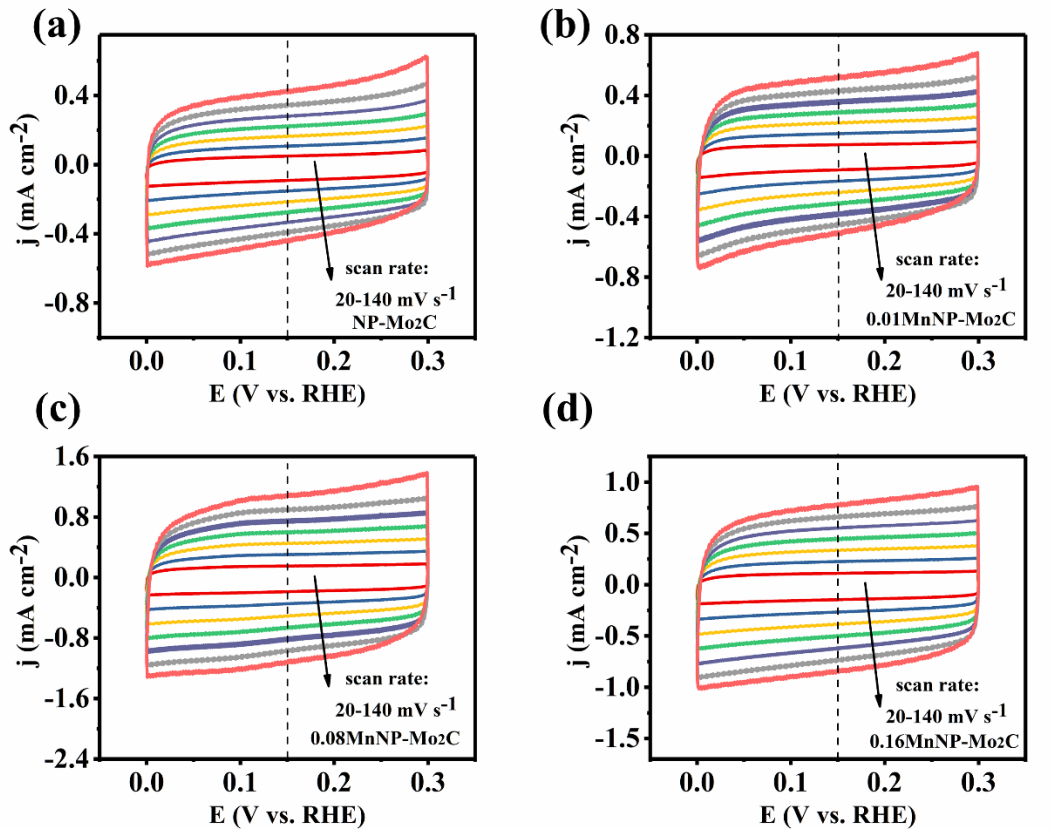

Fig. S3 CV curves of various samples in 0.5 M H_2SO_4: (a) NP-Mo_2C; (b) 0.01MnNP-Mo_2C; (c) 0.08NPMn-Mo_2C; (d) 0.16MnNP-Mo_2C.

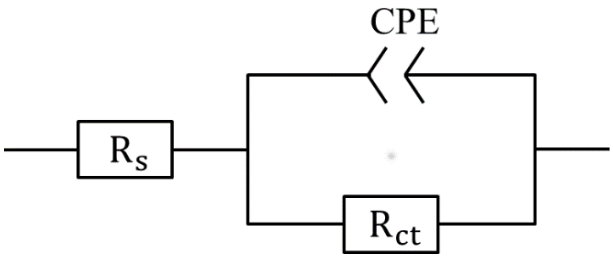

Fig. S4 Randles equivalent circuit model for electrochemical impedance tests.

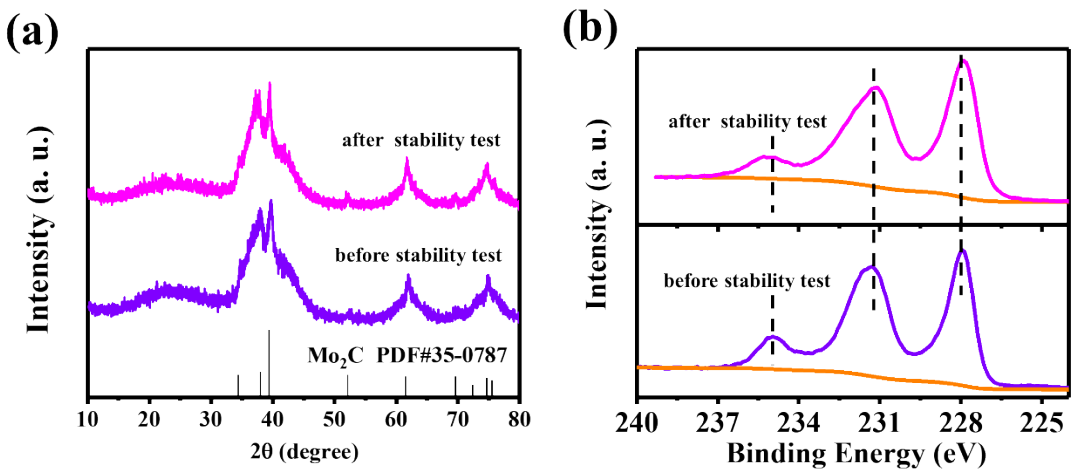

Fig. S5 (a) XRD patterns and (b) XPS spectra of 0.08MnNP-Mo_2C before and after stability test.

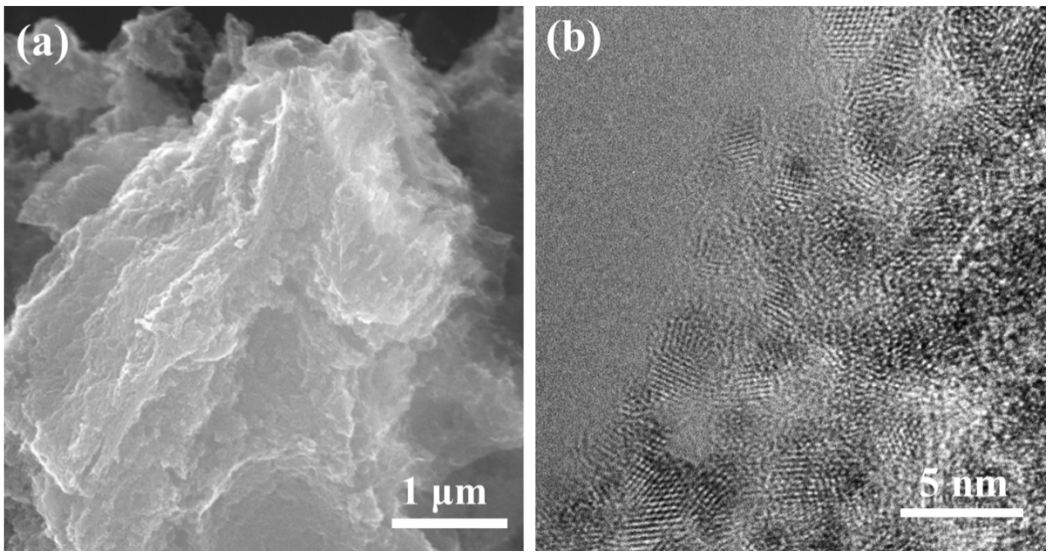

Fig. S6 (a) SEM and (b) TEM images of the 0.08MnNP-Mo_2C after the long-time stability test.

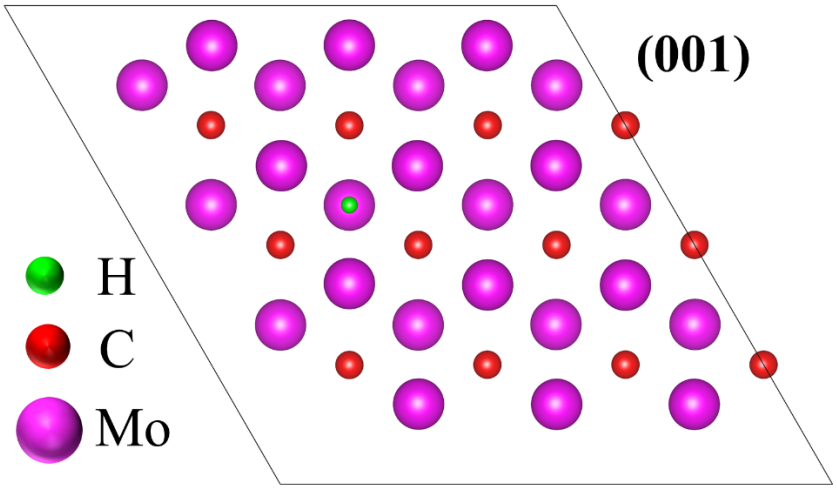

Fig. S7 Theoretical structural model of pure Mo_2C with the stable adsorption of H* on Mo site.

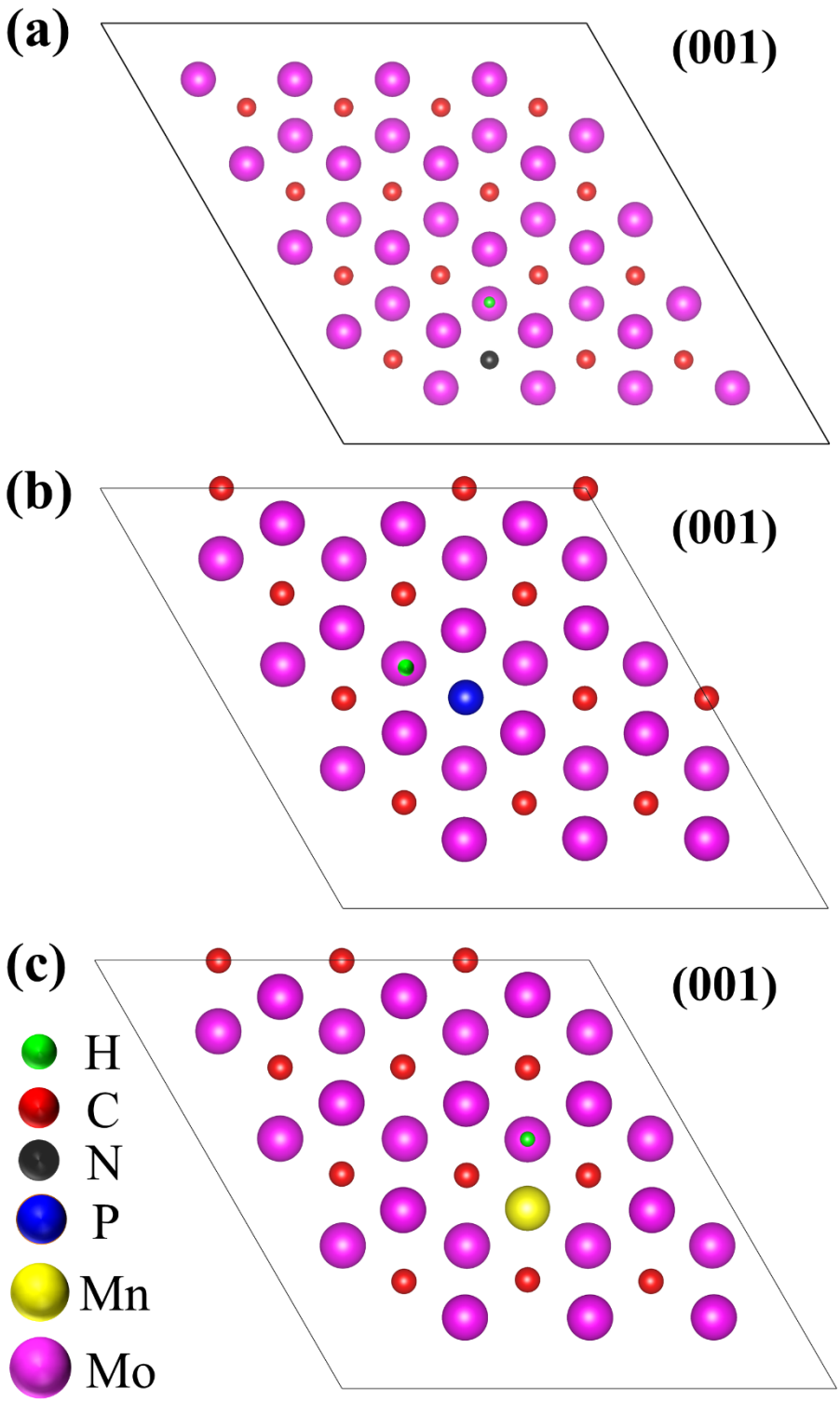

Fig. S8 Theoretical structural models of (a) N doped Mo_2C, (b) P doped Mo_2C and (c) Mn doped Mo_2C with the stable adsorption of H* on Mo site.

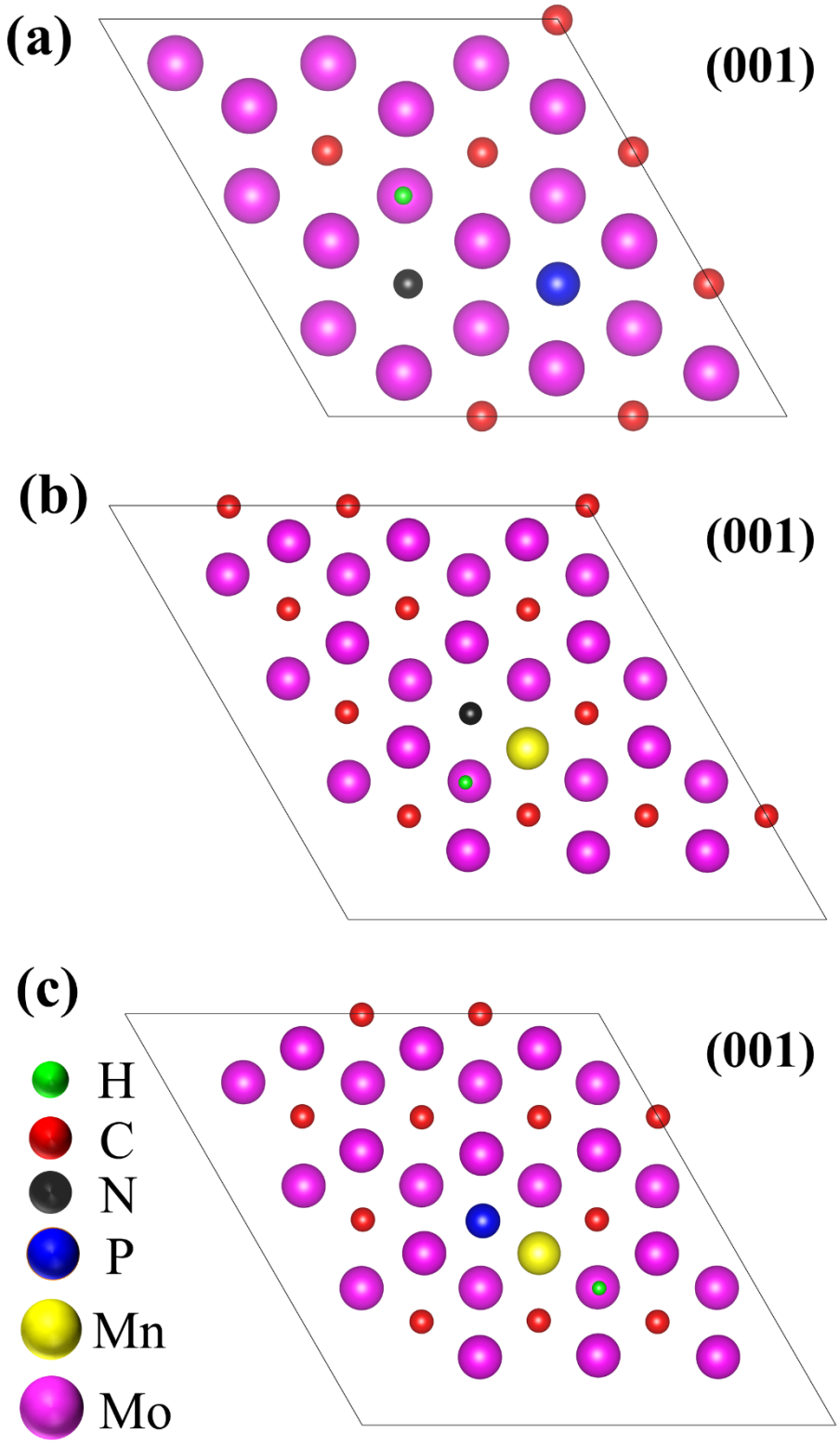

Fig. S9 Theoretical structural models of (a) N, P co-doped Mo_2C, (b) Mn, N co-doped Mo_2C and (c) Mn, P co-doped Mo_2C with the stable adsorption of H* on Mo site.

Table S4 Calculated Gibbs free energies (ΔG_{H^*}) for H adsorption on the Mo site in each atomic model.

Model	$\triangle G_{H^*}$ (eV) on the Mo site
pure Mo_2C	-0.4838
Model-N-Mo_2C (N doped Mo_2C model)	-0.5516
Model-P-Mo_2C (P doped Mo_2C model)	-0.4661
Model-Mn-Mo_2C (Mn doped Mo_2C model)	-0.8092
Model-NP-Mo_2C (N, P co-doped Mo_2C model)	-0.4101
Model-MnN-Mo_2C (Mn, N co-doped Mo_2C model)	-0.3510
Model-MnP-Mo_2C (Mn, P co-doped Mo_2C model)	-0.4493
Model-MnNP-Mo_2C (Mn, N and P co-doped Mo_2C model)	-0.1697

References

1 J. Kibsgaard and T. F. Jaramillo, *Angew. Chemie Int. Ed.*, 2014, **53**, 14433–14437.

2 T. Wang, X. Liu, S. Wang, C. Huo, Y.-W. Li, J. Wang and H. Jiao, *J. Phys. Chem. C*, 2011, **115**, 22360–22368.

3 J. K. Nørskov, T. Bligaard, A. Logadottir, J. R. Kitchin, J. G. Chen, S. Pandelov and U. Stimming, *J. Electrochem. Soc.*, 2005, **152**, J23–J26.

4 Y. Zhou, J. Xu, C. Lian, L. Ge, L. Zhang, L. Li, Y. Li, M. Wang, H. Liu and Y. Li, *Inorg. Chem. Front.*, 2019, **6**, 2464–2471.

5 H. Yan, Y. Xie, Y. Jiao, A. Wu, C. Tian, X. Zhang, L. Wang and H. Fu, *Adv. Mater.*, 2018, **30**, 1704156–1704163.

6 D. H. Youn, S. Han, J. Y. Kim, J. Y. Kim, H. Park, S. H. Choi and J. S. Lee, *ACS Nano*, 2014, **8**, 5164–5173.

7 J. Dong, Q. Wu, C. Huang, W. Yao and Q. Xu, *J. Mater. Chem. A*, 2018, **6**, 10028–10035.

8 X. Fan, Y. Liu, Z. Peng, Z. Zhang, H. Zhou, X. Zhang, B. I. Yakobson, W. A. Goddard, X. Guo, R. H. Hauge and J. M. Tour, *ACS Nano*, 2017, **11**, 384–394.

9 H. Lin, N. Liu, Z. Shi, Y. Guo, Y. Tang and Q. Gao, *Adv. Funct. Mater.*, 2016, **26**, 5590–5598.

10 Q. Liang, H. Jin, Z. Wang, Y. Xiong, S. Yuan, X. Zeng, D. He and S. Mu, *Nano Energy*, 2019, **57**, 746–752.

11 Z. Cheng, Q. Fu, Q. Han, Y. Xiao, Y. Liang, Y. Zhao and L. Qu, *Adv. Funct. Mater.*, 2018, **28**, 1705967–1705974.

12 Z. Kou, T. Wang, Y. Cai, C. Guan, Z. Pu, C. Zhu, Y. Hu, A. M. Elshahawy, J. Wang and S. Mu, *Small Methods*, 2018, **2**, 1700396–1700402.

13 C. Wu and J. Li, *ACS Appl. Mater. Interfaces*, 2017, **9**, 41314–41322.

14 Z. Shi, K. Nie, Z.-J. Shao, B. Gao, H. Lin, H. Zhang, B. Liu, Y. Wang, Y. Zhang, X. Sun, X.-M. Cao, P. Hu, Q. Gao and Y. Tang, *Energy Environ. Sci.*, 2017, **10**, 1262–1271.

15 Y.-Y. Chen, Y. Zhang, W.-J. Jiang, X. Zhang, Z. Dai, L.-J. Wan and J.-S. Hu, *ACS Nano*, 2016, **10**, 8851–8860.

16 T. Guo, X. Zhang, T. Liu, Z. Wu and D. Wang, *Appl. Surf. Sci.*, 2020, **509**, 144879–144886.

17 L. Liao, S. Wang, J. Xiao, X. Bian, Y. Zhang, M. D. Scanlon, X. Hu, Y. Tang, B. Liu and H. H. Girault, *Energy Environ. Sci.*, 2014, **7**, 387–392.